A Lyapunov Optimization Framework for Green Satellite Communications

Qilu Wu
Shenzhen MSU-BIT University
Shenzhen, China
Email: wuqilu0710@gmail.com

Xiaoyi Fan
Shenzhen MSU-BIT University
Shenzhen, China
Email: xiaoyi.fan@smbu.edu.cn

Zhen Zhang
Lanzhou University
Lanzhou, China
Email: zhangzhen19@lzu.edu.cn

Yang Zhou
Nova Stella (Shenzhen) Technology, Ltd
Shenzhen, China
Email: zhouyang@novastella.com.cn

Yike Li
Shenzhen MSU-BIT University
Shenzhen, China
Email: liyike@smbu.edu.cn

Haihan Duan
Shenzhen MSU-BIT University
Shenzhen, China
Email: duanhaihan@smbu.edu.cn

2025 IEEE International Conference on Cloud Computing Technology and Science (CloudCom) | 979-8-3315-6634-0/25/$31.00 ©2025 IEEE | DOI: 10.1109/CLOUDCOM67567.2025.11331549

***Abstract*—Satellite communication plays a crucial role in future networks, but traditional systems face significant challenges in interference management and energy efficiency. To address these issues, this paper proposes a green satellite communication framework that combines Lyapunov optimization with a one-dimensional golden-section search method. The framework builds a two-timescale frame-slot model that jointly captures fast-varying channel fading and slow-varying renewable energy dynamics. By introducing a drift-plus-penalty optimization method, the system ensures queue stability and minimizes long-term grid energy expenditure, while employing the golden-section search to optimize beamforming parameters with reduced computational complexity. Simulation results show that the proposed framework effectively balances energy efficiency and communication performance, demonstrating good scalability for large-scale satellite networks.**

***Index Terms*—Green communication, Lyapunov optimization, two-timescale modeling, energy efficiency**

I. Introduction

With the rapid acceleration of global digitalization, satellite communication has become a crucial component of modern society. It provides critical connectivity for remote areas, maritime operations, aviation, and other underserved regions, serving as a cornerstone for global data transmission and internet access [1]–[3]. As we transition from Fifth Generation (5G) to Sixth Generation (6G) networks, satellite communication is expected to play an increasingly significant role in meeting the demanding requirements of high throughput, low latency, and massive connectivity [4]–[7].

However, the growth in communication demands poses substantial challenges for traditional satellite systems, particularly in terms of interference management and energy efficiency [1], [2]. The surge in bandwidth demand and the growing number of connected devices, driven by data-intensive applications like high-definition video streaming and the Internet of Things (IoT), make it imperative to achieve higher throughput and lower latency [8]–[11]. Furthermore, the increasing number of user devices, especially in domains like remote sensing, maritime communication, and aviation, introduces additional complexities in interference management [12]–[15].

Haihan Duan is the corresponding author (duanhaihan@smbu.edu.cn).

A significant issue with conventional satellite communication systems is their high energy consumption [16]. lthough high-frequency bands, such as the Ka-band, enable fast data transmission, they also incur considerable energy costs. The energy required for satellite launch, maintenance, and operation imposes heavy financial and environmental burdens. In the context of 5G and the future 6G networks, reducing energy consumption and improving energy efficiency have become urgent research objectivess [17], [18]. Achieving a balance between communication performance and energy efficiency is thus a critical challenge for future satellite systems.

A. Related Works and Motivations

Several research efforts have been dedicated to addressing the challenges of bandwidth demand and interference in satellite communication. Classical methods such as frequency reuse, power control, and beamforming techniques have been employed to mitigate inter-beam interference [2], [19]. For example, frequency reuse schemes and adaptive power allocation have been shown to reduce interference between beams, while linear precoding methods, such as zero-forcing (ZF) and minimum mean-square error precoding, have been explored to improve signal quality and spectral efficiency [18], [20]–[22]. More recent advancements include optimization frameworks and machine learning-based algorithms designed to further enhance resource allocation and interference suppression [23]–[26]. However, these methods often treat each beam independently, limiting their effectiveness in highly coupled interference scenarios across multiple beams.

In terrestrial cellular networks, coordinated multi-point (CoMP) has been extensively investigated as an effective interference mitigation technique [22], [27]–[29]. CoMP enables multiple transmission points to cooperate, thereby improving capacity, coverage, and user experience. Its typical implementations include coordinated scheduling/beamforming, joint transmission, and dynamic point selection [17], [22], [30],

[31]. Inspired by its success in 4G/5G networks, researchers have begun exploring the feasibility of applying CoMP to satellite systems [2]. In geostationary earth orbit (GEO) satellites, CoMP-like beam coordination can reduce inter-beam interference, while in low earth orbit (LEO) constellations, inter-satellite cooperation can further enhance system performance [32], [33]. Nevertheless, these studies remain in the early stage, and the practical challenges of long propagation delays, limited inter-satellite links, and onboard processing constraints remain largely unresolved [34], [35].

Parallel to interference management, energy efficiency has become another key concern in satellite communication [8], [36], [37]. Existing works have studied power optimization strategies, satellite payload energy management, and the use of renewable energy sources such as solar power to reduce reliance on ground-based energy. In addition, green communication concepts from terrestrial networks have been extended to satellites, emphasizing metrics such as energy per bit and lifetime-aware optimization [38], [39]. While these studies highlight the importance of sustainable satellite operations, they often neglect the strong coupling between interference mitigation and energy consumption.

B. Our Contribution

The key contributions of this paper are summarized as follows:

- **Cross-timescale modeling:** We develop a frame–slot two-timescale model that couples fast channel dynamics with slow renewable-energy availability, and explicitly incorporates smart-grid buy/sell interactions ($c_b > c_s$), enabling a clean separation between slow and fast decisions for green satellite communication.
- **Lyapunov-based green optimization:** We cast long-term grid-energy expenditure minimization under queueing constraints into a drift-plus-penalty formulation with a frame-level drift bound and a per-slot deterministic objective $J_t(\varphi)$ that jointly governs scheduling, beamforming, and grid transactions, yielding queue-stability guarantees.
- **LONE: low-complexity beamforming with validated scalability and gains:** We integrate Lyapunov control with a golden-section one-dimensional search on the beamforming parameter φ, achieving per-slot complexity $\mathcal{O}(LN\log(\Delta/\tau))$ and $\mathcal{O}(1)$ extra space, thus scaling with antennas L and users N. Extensive evaluations against Zero-Forcing beamforming (ZFBF) across different V, renewable levels, and grid prices show consistently lower average grid-energy cost while maintaining stable end-to-end delay, delivering a more balanced energy–delay trade-off.

C. Organization

The remainder of this paper is organized as follows. Section II introduces the system architecture, including the network model, channel model, energy model, and traffic queues. Section III presents the proposed optimization framework that integrates Lyapunov optimization with a one-dimensional golden-section search. Section IV provides the simulation setup, performance evaluation, and discussion of the key results. Section V concludes the paper and outlines future research directions.

II. System Architecture

A. Network Architecture and Time Structure

We consider a single-satellite multi-user communication system, where one satellite provides direct connectivity to N terrestrial user equipments (UEs). The satellite is equipped with an array of L antennas, forming a multiple-input single-output downlink system. It can simultaneously serve multiple UEs by employing beamforming techniques. The satellite is powered by renewable energy sources (e.g., solar energy) with onboard battery storage, and is further supported by a bidirectional energy trading interface with the terrestrial smart grid. There are N single-antenna UEs randomly distributed within the satellite's coverage area, and each UE requests downlink transmission while providing channel state information (CSI) feedback to the satellite.

To capture both fast-varying channel dynamics and the slow-varying energy processes, the system adopts a two-timescale hierarchical structure composed of frames and slots. Each frame is indexed by $k \in \{0, 1, 2, \dots\}$ and has a duration of T_f. A frame consists of S consecutive slots, each with duration T_s, such that $T_f = S \cdot T_s$. Slots within frame k are indexed by $t \in \mathcal{T}_k = \{kS + 1, \dots, (k+1)S\}$. The two-timescale coordination enables the system to adapt beamforming to fast channel variations while maintaining long-term scheduling and energy sustainability, which reduces complexity, improves stability, and aligns with practical system operations.

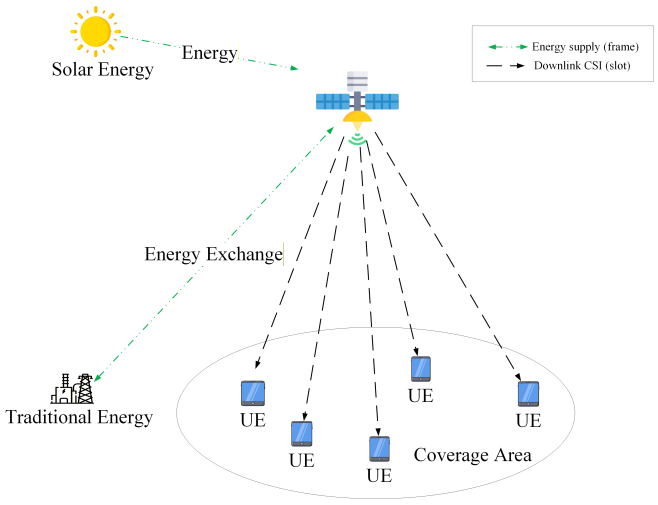

Fig. 1. Illustration of the single-satellite multi-user communication system with renewable energy supply and two-timescale frame-slot structure.

B. Channel Model

The satellite-UE downlink channel is modeled as a block-fading Rayleigh channel. Specifically, the channel remains constant within each time slot but independently changes

across different slots. Let $\mathbf{h}_n(t) \in \mathbb{C}^{L\times 1}$ denote the channel vector from the satellite to UE $n \in \{1,\dots,N\}$ at slot t. We assume that $\mathbf{h}_n(t) \sim \mathcal{CN}(\mathbf{0},\mathbf{I})$, where $\mathcal{CN}(\mathbf{0},\mathbf{I})$ denotes a circularly symmetric complex Gaussian distribution with zero mean and identity covariance matrix, implying independent and identically distributed (i.i.d.) Rayleigh fading across the L antennas.

The scheduling decision for each UE n at each frame k is represented by the binary decision variable $x_n[k]$, where:

$$x_n[k] = \begin{cases} 1, & \text{if UE } n \text{ is scheduled in frame } k, \\ 0, & \text{otherwise.} \end{cases} \tag{1}$$

The received signal of UE n at slot t is given by:

$$\begin{aligned} y_n(t) =& \sqrt{x_n[k]}\mathbf{h}_n^H(t)\mathbf{w}_n(t)s_n(t) \\ &+ \sum_{i\in\mathcal{S}_k, i\neq n} \sqrt{x_i[k]}\mathbf{h}_n^H(t)\mathbf{w}_i(t)s_i(t) + z_n(t). \end{aligned} \tag{2}$$

where $\mathbf{w}_i(t)$ is the beamforming vector for UE i, $\mathcal{S}_k$ denotes the set of scheduled UEs in frame k, $s_i(t)$ is the transmitted symbol with $\mathbb{E}[|s_i(t)|^2] = 1$ and $z_n(t) \sim \mathcal{CN}(0,\sigma^2)$ denotes the additive white Gaussian noise (AWGN). Here, σ^2 represents the noise power of a single complex baseband sample.

Accordingly, the signal-to-interference-plus-noise ratio (SINR) of UE n at slot t can be expressed as:

$$\mathrm{SINR}_n(t) = \frac{x_n[k]|\mathbf{h}_n^H(t)\mathbf{w}_n(t)|^2}{\sum\limits_{i\in\mathcal{S}_k, i\neq n} x_i[k]|\mathbf{h}_n^H(t)\mathbf{w}_i(t)|^2 + \sigma^2}. \tag{3}$$

Remark 1: We assume that the transmitted symbols are normalized such that $\mathbb{E}[|s_i(t)|^2] = 1$. This assumption does not affect generality but simplifies the analysis, since the transmit power is fully captured by the beamforming vectors.

Treating multiuser interference as noise, the per-slot spectral efficiency of UE n is $r_n(t) = \log_2\big(1 + \mathrm{SINR}_n(t)\big)$, and the instantaneous rate over bandwidth B is $R_n(t) = B\, r_n(t) = B\, \log_2\big(1 + \mathrm{SINR}_n(t)\big)$.

The satellite's instantaneous transmit power in slot t is determined by the beamforming vectors:

$$P_{\mathrm{tx}}(t) = \sum_{n\in\mathcal{S}_k} \big\|\mathbf{w}_n(t)\big\|_{\mathrm{F}}^2. \tag{4}$$

The communication payload power consumption is modeled as $P_{\mathrm{comm}}(t) = \frac{1}{\eta_{\mathrm{PA}}} P_{\mathrm{tx}}(t) + P_{\mathrm{c}}$, where $\eta_{\mathrm{PA}} \in (0,1]$ denotes the power amplifier efficiency, and P_{c} collects power terms that are independent of the instantaneous transmit power (e.g., baseband processing and Radio Frequency chains). When beamforming is optimized without explicitly pricing energy in the objective, we enforce a transmit-power constraint:

$$\sum_{n} \big\|\mathbf{w}_n(t)\big\|_{\mathrm{F}}^2 \le P^{\max} \tag{5}$$

where $P^{\max}$ denotes the per-slot total transmit power budget of the satellite payload.

C. Energy Model

The harvested energy $H[k]$ during each frame k is proportional to the total harvested energy. The energy harvested in each slot t within frame k is given by $H_t = \frac{1}{S} \cdot H[k]$. This allows each slot to receive a fraction of the total harvested energy proportional to the slot duration

The energy bought from and sold to the grid in slot t is calculated as [17]:

$$\begin{aligned} E_b[k] &= S \cdot \max\left\{P_{\mathrm{comm}}(t) - H_t, 0\right\}, \\ E_s[k] &= S \cdot \max\left\{H_t - P_{\mathrm{comm}}(t), 0\right\}. \end{aligned} \tag{6}$$

where$E_b[k]$ is the energy bought from the grid in slot t, $E_s[k]$ is the energy sold to the grid in slot t. The energy trading cost for frame k is then:

$$C_{\mathrm{grid}}[k] = (c_b - c_s)\, E_b[k] + c_s\, E_s[k], \tag{7}$$

where c_b is the constant price to buy energy from the grid, c_s is the constant price to sell energy to the grid. And $c_b > c_s > 0$, which ensures that the buying price c_b is always greater than the selling price c_s, thereby preventing arbitrage.

D. Traffic Model

The satellite maintains an access queue for each UE n. The dynamic equation for the n-th UE's access queue at slot k is given by:

$$Q_n^A(t+1) = Q_n^A(t) - r_n^A(t) + \nu_n^A(t), \tag{8}$$

where $Q_n^A(t)$ is the backlog of the access queue for UE n at slot t, $r_n^A(t)$ is the data rate at which UE n processes data in slot t, $\nu_n^A(t)$ is the data arrival rate of UE n in slot k.

The satellite also maintains a processing queue for each UE to handle upper layer processing. The dynamic equation for the n-th UE's processing queue is:

$$Q_n^U(t+1) = Q_n^U(t) - s_n^U(t) + r_n^U(t), \tag{9}$$

where $Q_n^U(t)$ is the backlog of the processing queue for UE n at slot k, $s_n^U(t) = \min\left(\tilde{s}_n^U, Q_n^U(t)\right)$ is the processing rate for UE n at slot k.

The arrival rate $\nu_n^A(t)$, data rate $r_n^A(t)$, and processing rate $s_n^U(t)$ are bounded by the following constraints [17]:

$$\nu_n^A(t) \in [0, \nu_{\max}], \quad r_n^A(t) \in [0, r_{\max}], \quad s_n^U(t) \in [0, s_{\max}]. \tag{10}$$

The average arrival rate $\bar{\nu}_n^A(t)$ and average processing rate $\bar{s}_n^U$ are defined as:

$$\bar{\nu}_n^A(t) = \mathbb{E}[\nu_n^A(t)], \quad \bar{s}_n^U(t) = \mathbb{E}[s_n^U(t)]. \tag{11}$$

The arrival rate vector and processing rate vector are given by:

$$\nu(t) = \mathrm{vec}([\nu_n^A(t)]_{\forall n}), \quad s(t) = \mathrm{vec}([s_n^U(t)]_{\forall n}). \tag{12}$$

E. Problem Formulation

1) Objective Function: The objective of our work is to minimize the long-term grid energy expenditure $C_{\text{grid}}[k]$,while considering the scheduling decisions, beamforming, and energy exchange in the system. Additionally, we aim to maximize communication performance.

$$\min_{X} \lim_{S\to\infty} \frac{1}{T_f} \sum_{k=1}^{S} \mathbb{E}\{C_{\text{grid}}[k]\} \tag{13}$$

Where X is the set of decision variables, including scheduling decisions, power allocations, and energy transactions.

2) Constraints: 1. Transmission Rate Constraints: Each UE can only transmit at a rate that does not exceed the amount of data waiting in it's queue. This ensures that the system does not over-saturate any UE's capacity:

$$r_n(t) \le Q_n^A(t), \quad \forall n \tag{14}$$

2. Dynamic Proportional Rate Constraints: The system ensures that users with a larger data backlog receive a higher transmission rate. This proportional relationship balances the service rates based on each user's queue size:

$$\frac{r_n(t)}{r_i(t)} = \frac{Q_n^A(t)}{Q_i^A(t)}, \quad \forall n, i. \tag{15}$$

3. Slot-Level Power Constraints: The power used for beamforming within each slot should not exceed the maximum transmit power allowed for each base station. This is represented as:

$$\sum_{n} \|\mathbf{w}_n(t)\|_F^2 \le P^{\max}, \quad \forall n \tag{16}$$

4. Queue Stability Constraints: To ensure that data for all users is eventually processed and served in finite time, we impose a queue stability constraint:

$$\limsup_{K\to\infty} \frac{1}{K} \sum_{k=0}^{K-1} \mathbb{E}\left\{Q_n^A(t) + Q_n^U(t)\right\} < \infty, \quad \forall n \tag{17}$$

III. System Optimization with Lyapunov and One-Dimensional Search

We present a comprehensive system optimization method that integrates Lyapunov optimization with one-dimensional search to achieve optimal system performance in terms of energy efficiency and stability. The primary objective is to minimize grid energy expenditure while maintaining the stability of access and processing queues in the system.

A. Lyapunov Optimization for Queue Stability

By bounding the Lyapunov drift at the frame level and decomposing it into per-slot decision terms, the original long-term stochastic optimization is transformed into a sequence of slot-level deterministic problems [40]–[42].

Lyapunov optimization is employed to ensure the queue stability of the system. The technique minimizes the drift of a Lyapunov function, which is based on the backlogs of access and processing queues. The key goal is to balance energy efficiency and queue stability while minimizing delays and ensuring long-term performance.

To measure the system's state, the Lyapunov function $L[k]$ is defined as the sum of the squared backlogs of the access and processing queues:

$$L_n[k] = \frac{1}{2}\|Q_n^A[k]\|_F^2 + \frac{1}{2}\|Q_n^U[k]\|_F^2. \tag{18}$$

The function captures the energy or penalty associated with the system's state. By minimizing the function, we ensure that the system avoids overloading and excessive data backlogs, keeping the system stable.

The Lyapunov drift $\Delta L[k]$ is defined as the difference between the Lyapunov function at the current and next frames:

$$\Delta L_n[k] = L_n[k+1] - L_n[k]. \tag{19}$$

The drift represents how the system's state evolves from one frame to the next. The objective of Lyapunov optimization is to minimize this drift, which in turn ensure that the queues do not grow uncontrollably, avoiding system overload.

Through the queue dynamic equations, we can compute the upper bound of the Lyapunov drift. By introducing the drift-plus-penalty method, we not only minimize the drift but also incorporate the grid energy expenditure into the optimization. This method balances the trade-off between queue stability and energy efficiency.

The drift bound is formulated as:

$$\begin{aligned}\Delta L[k] \;\le\; & T\Psi + \sum_{n=1}^{N} Q_n^A[k] \left(\sum_{t\in\mathcal{T}_k} \nu_n(t) - \sum_{t\in\mathcal{T}_k} r_n(t)\right) \\ & + \sum_{n=1}^{N} Q_n^U[k] \left(\sum_{t\in\mathcal{T}_k} r_n(t) - \sum_{t\in\mathcal{T}_k} s_n(t)\right).\end{aligned} \tag{20}$$

where Ψ is a constant that represents the maximum data arrival rate and maximum processing rate of the system. The bound on the drift provides an upper limit on how the system's state can evolve, which is critical for controlling the queues' growth and optimizing energy consumption.

By introducing the drift-plus-penalty, the instantaneous optimization objective becomes:

$$\Delta L[k] + V\mathbb{E}\{C_{\text{grid}}[k]\}, \tag{21}$$

where $V > 0$ is a tunable control parameter balancing energy efficiency and queue stability.

B. One-Dimensional Search for Optimal Parameter Selection

In the system optimization process, one-dimensional search is employed to determine the optimal parameter $\varphi \in [\varphi_{\min}, \varphi_{\max}]$, which regulates power allocation and scheduling. The parameter affects the beamforming vectors $\mathbf{w}_n(t;\varphi)$. Accordingly, the SINR and achievable rate of UE n at slot t are given by:

$$\text{SINR}_n(t;\varphi) = \frac{x_n[k]\left|\mathbf{h}_n^H(t)\mathbf{w}_n(t;\varphi)\right|^2}{\sum\limits_{i\in\mathcal{S}_k,\, i\neq n} x_i[k]\left|\mathbf{h}_n^H(t)\mathbf{w}_i(t;\varphi)\right|^2 + \sigma^2}, \tag{22}$$

and

$$r_n(t;\varphi) = \log_2(1 + \mathrm{SINR}_n(t;\varphi)). \tag{23}$$

Given the queue states, the drift-plus-penalty objective at slot t can be expressed as:

$$J_t(\varphi) = V\, C_{\text{grid}}(t;\varphi) + \sum_{n=1}^{N} \left(Q_n^U[k] - Q_n^A[k]\right)\, r_n(t;\varphi) - \sum_{n=1}^{N} Q_n^U[k]\, s_n(t). \tag{24}$$

Since $J_t(\varphi)$ is unimodal with respect to φ, the golden-section search is employed to efficiently find the optimal parameter. At each iteration, two intermediate points are evaluated within the current interval, the objective function values $J_t(\varphi)$ are compared, and the search range is updated accordingly. This process repeats until the search interval length falls below a predefined threshold τ, and the final optimal value is obtained as:

$$\varphi^\star = \tfrac{1}{2}\big(\varphi_{\min} + \varphi_{\max}\big). \tag{25}$$

The one-dimensional search allows us to efficiently tune the beamforming parameters $\mathbf{w}_n(t;\varphi)$, ensuring that both energy consumption and queue stability are optimized. The final solution balances communication performance with energy efficiency, contributing to the green communication goals of the system.

C. LONE Algorithm: Lyapunov Optimization with One-Dimensional Search

Lyapunov optimization plays a pivotal role in ensuring system stability while simultaneously minimizing grid energy consumption, whereas one-dimensional search is employed to optimize power allocation and scheduling decisions. By integrating these two approaches, the proposed LONE algorithm guarantees queue stability through Lyapunov optimization, while one-dimensional search fine-tunes critical system parameters, thereby reducing grid energy consumption and enhancing overall performance.

This synergistic combination ultimately achieves the desired green communication objectives, optimizing both energy efficiency and system stability. Therefore, the final per-slot optimization reduces to finding the parameter $\varphi^\star$ that minimizes $J_t(\varphi)$, subject to the power constraint:

$$\varphi^\star = \arg \min_{\varphi \in [\varphi_{\min}, \varphi_{\max}]} J_t(\varphi) \quad \text{s.t.} \quad \sum_{n \in \mathcal{S}_k} \|w_n(t;\varphi)\|_2^2 \le P_{\max}. \tag{26}$$

Algorithm Complexity Analysis: We analyze the computational complexity of the proposed LONE procedure, which couples Lyapunov optimization with a one-dimensional (golden-section) search over $\varphi \in [\varphi_{\min}, \varphi_{\max}]$.

At each iteration, computing the Lyapunov function and its drift over N UEs requires $\mathcal{O}(N)$ time. If the inner updates take T_{opt} iterations per frame, this part costs $\mathcal{O}\big(N\, T_{\text{opt}}\big)$ time and $\mathcal{O}(N)$ space to store the access/processing queues.

Algorithm 1 LONE: Lyapunov Optimization with One-Dimensional Search

1: **Initialization:** Set initial values for queue backlogs $Q_n^A[k]$, $Q_n^U[k]$, channel coefficients $h_{m,n}(t)$, energy harvesting rates $E_m^{\text{HAV}}[t]$.
2: **for** each frame k **do**
3: **Step 1: Lyapunov Optimization for Queue Stability**
4: Initialize Lyapunov function $L_n[k]$
5: Compute drift $\Delta L_n[k]$
6: Minimize drift using Lyapunov drift bound to ensure queue stability.
7: **Step 2: One-Dimensional Search for Optimal Parameter Selection**
8: Initialize the search interval $[\varphi_{\min}, \varphi_{\max}]$ and tolerance τ.
9: **repeat**
10: Compute two intermediate points φ_1 and φ_2 using the golden ratio $\varphi = \frac{1+\sqrt{5}}{2}$.
11: Evaluate the drift-plus-penalty objective $J_t(\varphi)$ at φ_1 and φ_2.
12: Update the interval by discarding the sub-interval with the worse objective value.
13: **until** $|\varphi_{\min} - \varphi_{\max}| \le \tau$
14: Set the optimal parameter $\varphi^\star(t) = \frac{1}{2}(\varphi_{\min} + \varphi_{\max})$.
15: **Step 3: Combine Results**
16: Obtain optimal values for power allocation parameters $\varphi^\star(t)$ and scheduling decisions $a_{m,n}[k]$
17: **Output:** Optimal scheduling decisions $\{a_{m,n}[k]\}$ and optimal power allocation boundaries $\varphi^\star(t)$
18: **end for**

Let $\Delta = \varphi_{\max} - \varphi_{\min}$ be the initial interval length and τ the final tolerance. Golden-section search performs $\Theta\big(\log(\Delta/\tau)\big)$ iterations. Let C_{eval} denote the cost of evaluating the drift-plus-penalty objective $J_t(\varphi)$ once. In our implementation, $C_{\text{eval}} = \mathcal{O}(LN)$ because evaluating rates and penalties involves linear/quadratic forms over L antennas and N UEs with precomputed channel terms. Hence the search costs $\mathcal{O}\big(C_{\text{eval}} \log(\Delta/\tau)\big) = \mathcal{O}\big(LN\, \log(\Delta/\tau)\big)$. The space overhead of the line search is $\mathcal{O}(1)$ (a few scalars for endpoints and function values).

Thus, the per-frame time complexity is $\mathcal{O}\big(N\, T_{\text{opt}}\big) + \mathcal{O}\big(LN\, \log(\Delta/\tau)\big)$, and the space complexity is $\mathcal{O}(N)$. Compared with the ZFBF algorithm, which requires matrix inversion or pseudo-inverse computations of the channel matrix with a per-iteration cost on the order of $\mathcal{O}(LN^2)$ or $\mathcal{O}(L^3)$, the proposed LONE algorithm incurs substantially lower complexity. In particular, the complexity of ZFBF grows cubically with the number of antennas and quadratically with the number of users, which limits its practicality in large-scale systems. By contrast, LONE exhibits only linear dependence on the number of users and logarithmic dependence on the search precision, thereby offering superior scalability and computational efficiency in green communication scenarios.

IV. Simulation and Discussion

To evaluate the performance of the proposed scheduling, beamforming, and energy management framework, we consider a single-satellite communication scenario, which is a typical LEO system. The main simulation parameters are summarized in Table I. The satellite is equipped with 12 antennas and serves 8 UEs. The carrier frequency is set to $f_c = 30$GHz, and the orbital altitude is approximately 1000 km. The circuit power consumption is set to $P_c = 25$W.

The large-scale channel attenuation is modeled by the free-space path loss (FSPL) model, expressed as:

$$F_{\text{fspl}}(d, f) = 32.44 + 20\log_{10}(d_{\text{km}}) + 20\log_{10}(f_{\text{MHz}}) \text{ (dB)}, \quad (27)$$

where d_{km} is the slant range in kilometers and f_{MHz} is the carrier frequency in megahertz.

Each UE is allocated a bandwidth of B=10 MHz, and the additive white Gaussian noise power is fixed at $\sigma^2 = -99$ dBm. The maximum satellite transmit power is $P^{\max} = 100$ W with a power amplifier efficiency of $\eta = 0.25$. The renewable energy(NRE) harvested by the satellite is set to 300 W from solar sources. The energy consumption is calculated based on the power amplifier efficiency and fixed circuit power, while the energy exchanged with the grid is determined by the availability of renewable energy. The grid electricity price is modeled with a buy price of 1.6 per unit and a sell price of 0.6 per unit, capturing the asymmetry of purchasing and selling energy in practice.

TABLE I
Key Simulation Parameters for the Single-Satellite Scenario

Symbol	Value
Antennas	12
N	8
f_c	30 GHz
Orbit altitude	1000 km
B	10 MHz
σ^2	-99 dBm
$P_{\max}$	300 W
P_{cct}	25 W
η	0.25
ν	1.5 nats/slot/Hz
$s_{\max}$	8 nats/slot/Hz
Δt	1 ms, $\lvert\mathcal{T}_k\rvert = 5$
V	0.01, 0.1, 1
Renewable power	400 W
Buy price	1.6 (per unit)
Sell price	0.6 (per unit)
Simulation duration	10^3 frames

We consider the ZFBF algorithm as a benchmark. ZFBF designs transmission beams to eliminate inter-user interference in multi-user systems, thereby enhancing system capacity and spectral efficiency.

Figures 2 and 3 show the average grid-energy cost and the average end-to-end delay as functions of the iteration index for varying V, with NRE fixed at 400 W. For energy cost, LONE is consistently lower and less variable than ZFBF across the entire V range. At small V, the gap is sizable (e.g., ZFBF ranges from 100 to 200 whereas LONE ranges from 50 to 90). As V increases, the costs of both methods decrease and can enter the negative region, with LONE remaining lower and smoother throughout. For delay, ZFBF attains a slightly smaller value only at very small V (around 6 time slots), but its delay grows markedly with V toward 9 time slots. In contrast, LONE is less sensitive to V, staying near 6.3–6.5 time slots at small/medium V and rising to about 8 time slots at the largest V. Overall, except in the very small-V regime, LONE provides a more favorable energy–delay trade-off.

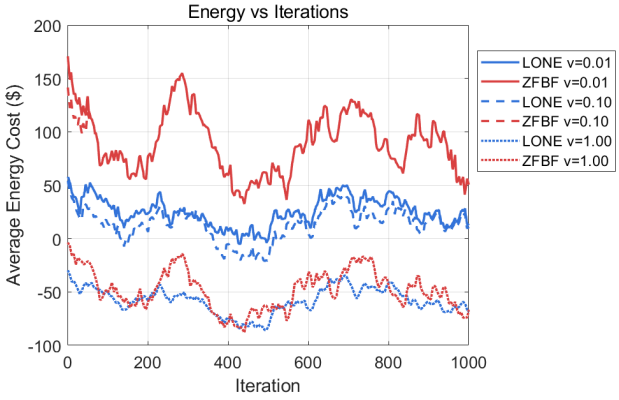

Fig. 2. Average energy cost iterations under different V values (NRE =400W).

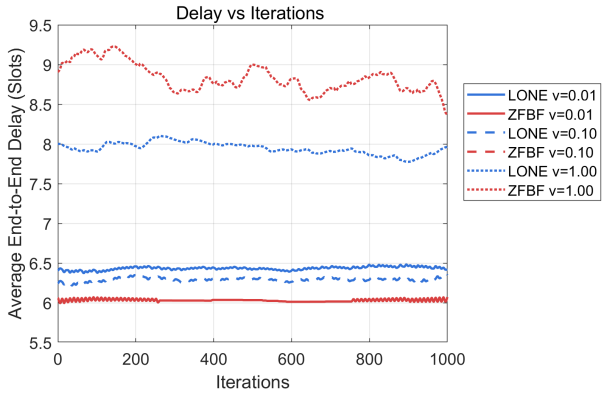

Fig. 3. Average end-to-end delay iterations under different V values (NRE =400W).

Figures 4 and 5 show the average grid-energy cost and the average end-to-end delay as functions of the iteration index for varying V, with NRE fixed at 300 W. For energy cost, LONE is consistently lower and less variable than ZFBF across the entire V range. At small V, the gap is sizable (e.g., ZFBF ranges from 100 to 200, whereas LONE ranges from 50 to 90.). As V increases, the costs of both methods decline and may enter the negative region; compared with the 400 W case, this region is less pronounced, and LONE remains lower and smoother throughout. For delay, ZFBF attains a smaller value only at very small V (around 6.0 time slots) but grows markedly with V toward 9–9.6 time slots. In contrast, LONE is less sensitive to V, staying near 6.3–6.5 time slots at small/medium V and rising to about 8 time slots at the largest V. Overall, except in the very small-V regime, LONE provides

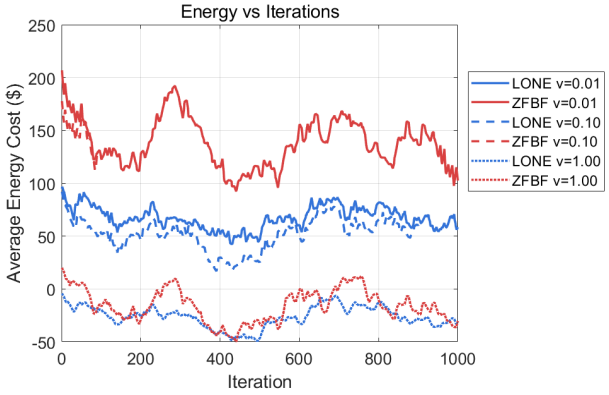

Fig. 4. Average energy cost iterations under different V values (NRE =300W).

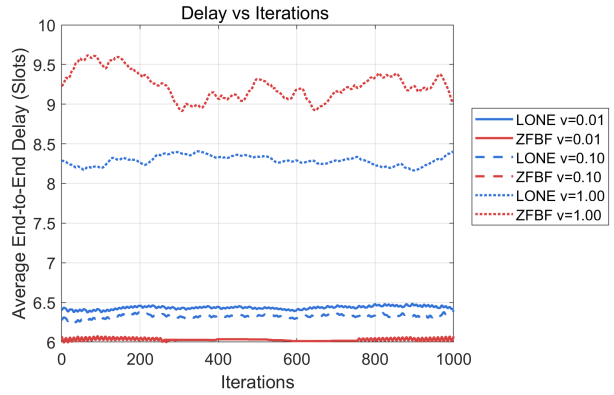

Fig. 5. Average end-to-end delay iterations under different V values (NRE =300W).

a more favorable energy–delay trade-off.

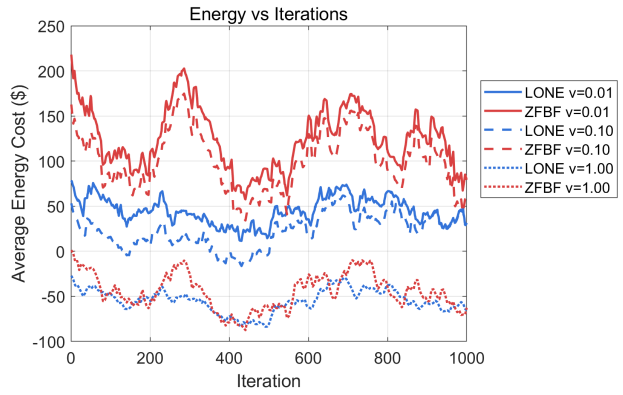

Fig. 6. Average energy cost versus iterations under different V values (buy price=2.0).

Figures 6 and 7 show the average grid-energy cost and the average end-to-end delay versus iterations for varying V, with the selling price set to 2 per unit. For energy cost, LONE is consistently lower and less variable than ZFBF across the entire V range. At small V, the gap is sizable (e.g., ZFBF ranges from 100 to 200 whereas LONE ranges from 50 to 90).

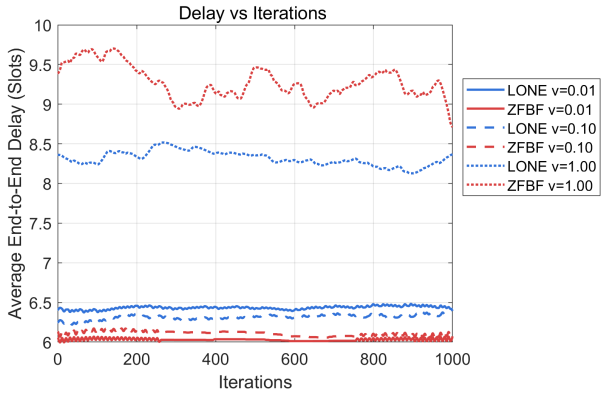

Fig. 7. Average end-to-end delay versus iterations under different V values (buy price=2.0).

As V increases, the costs of both methods decline and enter the negative region, which is enlarged by the higher selling price; within this region LONE remains more favorable (approximately $[-80, -40]$) than ZFBF (approximately $[-70, -20]$) and exhibits smoother trajectories. For delay, ZFBF attains a smaller value only at very small V (around 6.0–6.1 time slots) but grows markedly with V toward 9.0–9.6 time slots. In contrast, LONE is less sensitive to V, staying near 6.3–6.5 time slots at small/medium V and rising to about 8.2–8.5 time slots at the largest V. Overall, except in the very small-V regime, LONE provides a more favorable energy–delay trade-off.

V. Conclusion

This paper presents a green satellite communication framework that combines Lyapunov optimization with a one-dimensional search to manage interference and improve energy efficiency. A two-timescale model captures fast channel dynamics and slow renewable variations. Lyapunov control stabilizes queues while minimizing long-term grid energy use, and the one-dimensional search enables low-complexity, scalable beamforming. Simulations show a good balance between energy cost and communication performance, indicating strong practical potential.

Future research can focus on improving the Lyapunov optimization algorithm for better efficiency, expanding the framework to multi-satellite networks, and exploring machine learning-based methods to handle dynamic changes in communication and energy needs.

Acknowledgment

This work was supported in part by the National Natural Science Foundation of China (Grant No.62576213); and in part by Engineering Technology Research Center for Ordinary Universities in Guangdong Province (No.2024GCZX005); in part by Guangdong-Hong Kong-Macao Joint Laboratory for Emotional Intelligence and Pervasive Computing, Artificial Intelligence Research Institute, Shenzhen MSU-BIT University.

REFERENCES

[1] M. Á. Vázquez, A. Perez-Neira, D. Christopoulos, S. Chatzinotas, B. Ottersten, P.-D. Arapoglou, A. Ginesi, and G. Taricco, "Precoding in multibeam satellite communications: Present and future challenges," *IEEE Wireless Communications*, vol. 23, no. 6, pp. 88–95, 2016.

[2] A. Guidotti, A. Vanelli-Coralli, M. Conti, S. Andrenacci, S. Chatzinotas, N. Maturo, *et al.*, "Architectures and key technical challenges for 5g systems incorporating satellites," *IEEE Transactions on Vehicular Technology*, vol. 68, no. 3, pp. 2624–2639, 2019.

[3] G. Giambene, S. Kota, and P. Pillai, "Satellite-5g integration: A network perspective," *IEEE Network*, vol. 32, no. 5, pp. 25–31, 2018.

[4] O. Kodheli, E. Lagunas, N. Maturo, S. K. Sharma, B. Shankar, J. F. M. Montoya, J. C. M. Duncan, D. Spano, *et al.*, "Satellite communications in the new space era: A survey and future challenges," *IEEE Communications Surveys & Tutorials*, vol. 23, no. 1, pp. 70–109, 2021.

[5] M. Jia, X. Gu, Q. Guo, W. Xiang, and N. Zhang, "Broadband hybrid satellite-terrestrial communication systems based on cognitive radio toward 5g," *IEEE Wireless Communications*, vol. 23, no. 6, pp. 96–106, 2016.

[6] K. An, M. Lin, J. Ouyang, and W.-P. Zhu, "Secure transmission in cognitive satellite terrestrial networks," *IEEE Journal on Selected Areas in Communications*, vol. 34, no. 11, pp. 3025–3037, 2016.

[7] W. Jiang, "Software defined satellite networks: A survey," *Digital Communications and Networks*, vol. 9, no. 6, pp. 1243–1264, 2023.

[8] C. Qi, Y. Yang, R. Ding, S. Jin, and D. Liu, "Multibeam satellite communications with energy efficiency optimization," *IEEE Communications Letters*, vol. 26, no. 4, pp. 887–891, 2022.

[9] Z. Han, C. Xu, Z. Xiong, G. Zhao, and S. Yu, "On-demand dynamic controller placement in software defined satellite-terrestrial networking," *IEEE Transactions on Network and Service Management*, vol. 18, no. 3, pp. 2915–2928, 2021.

[10] Z. Shangguan, Y. Dong, S. Guo, V. Leung, M. J. Deen, and X. Hu, "Facial expression analysis and its potentials in iot systems: A contemporary survey," *arXiv preprint arXiv:2412.17616*, 2024.

[11] M. Yang, E. C. Ngai, X. Hu, B. Hu, J. Liu, E. Gelenbe, and V. C. Leung, "Digital phenotyping and feature extraction on smartphone data for depression detection," *Proceedings of the IEEE*, 2025.

[12] A. M.K. and M. R. Bhatnagar, "Beamforming and combining in hybrid satellite-terrestrial cooperative systems," *IEEE Communications Letters*, vol. 18, no. 3, pp. 483–486, 2014.

[13] K. An, M. Lin, T. Liang, J.-B. Wang, J. Wang, Y. Huang, and A. L. Swindlehurst, "Performance analysis of multi-antenna hybrid satellite-terrestrial relay networks in the presence of interference," *IEEE Transactions on Communications*, vol. 63, no. 11, pp. 4390–4404, 2015.

[14] K. An, J. Ouyang, M. Lin, and T. Liang, "Outage analysis of multi-antenna cognitive hybrid satellite-terrestrial relay networks with beamforming," *IEEE Communications Letters*, vol. 19, no. 7, pp. 1157–1160, 2015.

[15] T. Wei, W. Feng, Y. Chen, C.-X. Wang, N. Ge, and J. Lu, "Hybrid satellite-terrestrial communication networks for the maritime internet of things: Key technologies, opportunities, and challenges," *IEEE Internet of Things Journal*, vol. 8, no. 11, pp. 8910–8934, 2021.

[16] A. O.-O. Esho, T. D. Iluyomade, T. M. Olatunde, and O. P. Igbinenikaro, "A comprehensive review of energy-efficient design in satellite communication systems," *International Journal of Engineering Research Updates*, vol. 6, no. 02, pp. 013–025, 2024.

[17] Y. Dong, M. J. Hossain, J. Cheng, and V. C. M. Leung, "Cross-layer scheduling and beamforming in smart-grid powered cellular networks with heterogeneous energy coordination," *IEEE Transactions on Communications*, vol. 68, no. 5, pp. 2711–2725, 2020.

[18] R. Martin, "Speech enhancement based on minimum mean-square error estimation and supergaussian priors," *IEEE Transactions on Speech and Audio Processing*, vol. 13, no. 5, pp. 845–856, 2005.

[19] Y. Dong, L. Wang, J. Wang, X. Hu, H. Zhang, F. R. Yu, and V. C. M. Leung, "Accelerating wireless federated learning via nesterov's momentum and distributed principal component analysis," *IEEE Transactions on Wireless Communications*, vol. 23, no. 6, pp. 5938–5952, 2024.

[20] A. Wiesel, Y. C. Eldar, and S. Shamai, "Zero-forcing precoding and generalized inverses," *IEEE Transactions on Signal Processing*, vol. 56, no. 9, pp. 4409–4418, 2008.

[21] Y. Yang and R. S. Blum, "Mimo radar waveform design based on mutual information and minimum mean-square error estimation," *IEEE Transactions on Aerospace and Electronic Systems*, vol. 43, no. 1, pp. 330–343, 2007.

[22] Y. Dong, H. Zhang, J. Li, F. R. Yu, S. Guo, and V. C. M. Leung, "An online zero-forcing precoder for weighted sum-rate maximization in green comp systems," *IEEE Transactions on Wireless Communications*, vol. 21, no. 9, pp. 7566–7581, 2022.

[23] T. Chen, Q. Ling, and G. B. Giannakis, "Learn-and-adapt stochastic dual gradients for network resource allocation," *IEEE Transactions on Control of Network Systems*, vol. 5, no. 4, pp. 1941–1951, 2018.

[24] X. Wang, X. Chen, T. Chen, L. Huang, and G. B. Giannakis, "Two-scale stochastic control for integrated multipoint communication systems with renewables," *IEEE Transactions on Smart Grid*, vol. 9, no. 3, pp. 1822–1834, 2018.

[25] T. Chen, Q. Ling, and G. B. Giannakis, "Online convex optimization for dynamic network resource allocation," in *2017 25th European Signal Processing Conference (EUSIPCO)*, pp. 136–140, 2017.

[26] Y. Dong, H. Zhang, C. Li, S. Guo, V. Leung, and X. Hu, "Fine-tuning and deploying large language models over edges: Issues and approaches," *arXiv preprint arXiv:2408.10691*, 2024.

[27] S. Brueck, L. Zhao, J. Giese, and M. A. Amin, "Centralized scheduling for joint transmission coordinated multi-point in lte-advanced," in *2010 International ITG Workshop on Smart Antennas (WSA)*, pp. 177–184, 2010.

[28] Q. Wu, Y. Dong, X. Fan, X. Hu, B. Hu, and V. C. Leung, "A carbon-neutralized comp with energy-sharing: A learn-and-adapt approach," *IEEE Internet of Things Journal*, pp. 1–1, 2025.

[29] V. C. M. Leung, Y. Dong, and H. Pan, "Editorial recent techniques of green information and communications technologies," *IEEE Transactions on Green Communications and Networking*, vol. 5, no. 4, pp. 1649–1652, 2021.

[30] T. Chen, Q. Ling, and G. B. Giannakis, "Learn-and-adapt network resource allocation," in *2017 IEEE 18th International Workshop on Signal Processing Advances in Wireless Communications (SPAWC)*, pp. 1–5, 2017.

[31] Y. Shen, T. Chen, and G. B. Giannakis, "Online learning adaptive to dynamic and adversarial environments," in *2018 IEEE 19th International Workshop on Signal Processing Advances in Wireless Communications (SPAWC)*, pp. 1–5, 2018.

[32] K.-U. Storek and A. Knopp, "Fair user grouping for multibeam satellites with mu-mimo precoding," in *GLOBECOM 2017 - 2017 IEEE Global Communications Conference*, pp. 1–7, 2017.

[33] V. Bankey and P. K. Upadhyay, "Ergodic capacity of multiuser hybrid satellite-terrestrial fixed-gain af relay networks with cci and outdated csi," *IEEE Transactions on Vehicular Technology*, vol. 67, no. 5, pp. 4666–4671, 2018.

[34] M. Beyaz, "Satellite communications with 5g, b5g, and 6g: challenges and prospects," *International Journal of Communications, Network and System Sciences*, vol. 17, no. 3, pp. 31–49, 2024.

[35] P. K. Sharma, D. Deepthi, and D. I. Kim, "Outage probability of 3-d mobile uav relaying for hybrid satellite-terrestrial networks," *IEEE Communications Letters*, vol. 24, no. 2, pp. 418–422, 2020.

[36] C. Qi, H. Chen, Y. Deng, and A. Nallanathan, "Energy efficient multicast precoding for multiuser multibeam satellite communications," *IEEE Wireless Communications Letters*, vol. 9, no. 4, pp. 567–570, 2020.

[37] C. Qi and X. Wang, "Precoding design for energy efficiency of multi-beam satellite communications," *IEEE Communications Letters*, vol. 22, no. 9, pp. 1826–1829, 2018.

[38] Q. Huang, M. Lin, W.-P. Zhu, S. Chatzinotas, and M.-S. Alouini, "Performance analysis of integrated satellite-terrestrial multiantenna relay networks with multiuser scheduling," *IEEE Transactions on Aerospace and Electronic Systems*, vol. 56, no. 4, pp. 2718–2731, 2020.

[39] Y. Xu, Y. Wang, R. Sun, and Y. Zhang, "Joint relay selection and power allocation for maximum energy efficiency in hybrid satellite-aerial-terrestrial systems," in *2016 IEEE 27th Annual International Symposium on Personal, Indoor, and Mobile Radio Communications (PIMRC)*, pp. 1–6, 2016.

[40] M. Neely, *Stochastic network optimization with application to communication and queueing systems*. Morgan & Claypool Publishers, 2010.

[41] P. Robert, *Stochastic networks and queues*, vol. 52. Springer Science & Business Media, 2013.

[42] Y. Mao, J. Zhang, and K. B. Letaief, "A lyapunov optimization approach for green cellular networks with hybrid energy supplies," *IEEE Journal on Selected Areas in Communications*, vol. 33, no. 12, pp. 2463–2477, 2015.